Available online at www.sciencedirect.com

ScienceDirect

Procedia Structural Integrity 21 (2019) 2–11

Structural Integrity Procedia

www.elsevier.com/locate/procedia

1st International Workshop on Plasticity, Damage and Fracture of Engineering Materials

Experimental Investigation of Crack Propagation Mechanisms in Commercially Pure Aluminium Plates

C. Tekoğlu[a,*], Ş. Çelik[a], H. Duran[b], M. Efe[c], K. L. Nielsen[d]

[a]*Department of Mechanical Engineering, TOBB University of Economics and Technology, Söğütözü, Ankara 06560, Turkey*

[b]*Department of Materials Science and Nanotechnology Engineering, TOBB University of Economics and Technology, Söğütözü, Ankara 06560, Turkey*

[c]*Department of Metallurgical and Materials Engineering, Middle East Technical University, Ankara 06800, Turkey*

[d]*Department of Mechanical Engineering, Solid Mechanics, Technical University of Denmark, DK-2800 Kgs. Lyngby, Denmark*

Abstract

The crack surface morphology in tearing of ductile metal plates depends on the mechanical properties, chemical composition and the microstructure of the plate material as well as on the loading conditions and the specimen geometry. This study assesses the crack surface morphologies observed in commercially pure aluminium plates (Al 1050 H14). Mode I tearing was performed in both single and double edge notched tensile test setups with specimens cut from five different plates with different thickness t, viz. $t \in \{0.5, 1, 3, 4, 5\}$ mm. In each combination, the long axis of the notch was either parallel (0°) or perpendicular (90°) to the rolling direction. Fractographs showed that, for specimen thicknesses smaller than 5 mm, the crack had a cup-cup morphology almost throughout its entire length for 0° specimens, while slanted crack propagation was visible in some regions of 90° specimens. For $t = 5$ mm, on the other hand, the dominant crack morphology was slanted for both directions, the extent of the cup-cup regions being larger for 0° specimens. The crack morphologies were repeatable for each direction-thickness combination, while also being consistent for both test setups having different loading conditions.

© 2019 The Authors. Published by Elsevier B.V.
This is an open access article under the CC BY-NC-ND license (http://creativecommons.org/licenses/by-nc-nd/4.0/)
Peer-review under responsibility of the 1st International Workshop on Plasticity, Damage and Fracture of Engineering Materials organizers

Keywords: Ductile failure; Plate tearing; Crack propagation

1. Introduction

Metal plates and shells enjoy superior properties such as high specific stiffness, specific strength, load carrying capacity, high degree of structural integrity, and low space requirement. They are therefore widely used as structural components in many branches of technology such as piping systems, pressure vessels, containment shells of nuclear

* Corresponding author. Tel.: +90-312-292-4065 ; fax: +90-312-292-4091.
E-mail address: cihantekoglu@etu.edu.tr

2452-3216 © 2019 The Authors. Published by Elsevier B.V.
This is an open access article under the CC BY-NC-ND license (http://creativecommons.org/licenses/by-nc-nd/4.0/)
Peer-review under responsibility of the 1st International Workshop on Plasticity, Damage and Fracture of Engineering Materials organizers
10.1016/j.prostr.2019.12.080

power plants, aircraft, exterior surfaces of missiles and rockets, ships, bridges, machine parts, etc. (see e.g. Ventsel and Krauthammer, 2001; Ugural, 2009). The mechanical properties of structural metallic alloys are continually improved such that cleavage and intergranular fracture mechanisms are mostly successfully avoided, leaving ductile fracture as the main failure mechanism upon overloading. Therefore, together with fatigue and corrosion, ductile fracture is the key ingredient in structural integrity assessment of metals (see e.g. Tekoğlu et al., 2015 a, and references therein).

The first stage of ductile fracture in metals and metal alloys is the nucleation of micron-scale voids, which occurs through either the fracture of second phase particles contained in the material, or the decohesion of the interface between the particles and the surrounding metal. With further loading, the nucleated (as well as possible pre-existing) voids grow, change shape, get closer to each other, and coalesce to form micro cracks. The micro cracks propagate and merge into macro cracks, which finally lead to the overall fracture of the material (see e.g. Lecarme et al., 2011; Pardoen et al., 2011; Scheyvaerts et al., 2011; Tekoğlu et al., 2010, 2012, 2015 b). This complex process forms the well-known cup-cone failure observed under uni-axial tension (Tvergaard and Needleman, 1984), with the elevated triaxiality in the centre of a diffuse neck fertilizing void growth that initiates a penny shape crack with fronts travelling toward the free surface. In a similar way, the propagation of a ductile tearing crack is highly influenced by the interplay between nucleation, growth, and coalescence of voids. Fig. 1 shows schematically the three experimentally observed crack propagation mechanisms in the ductile failure of metal plates: (a) slanted, (b) cup-cup, and (c) cup-cone crack growth (see e.g. El-Naaman and Nielsen, 2013). In real life applications, propagating tearing cracks usually show a mixture of the three different propagation modes. Fundamental books on fracture mechanics state that metal plates exhibit slanted crack propagation (see e.g. Knott, 1973; Anderson, 2005), which is indeed the case for plates made of high strength age-hardened aluminium alloys (see e.g. Irwin et al., 1958; Knott, 1973; Li and Siegmund, 2002), and of high strength steels (see e.g. Broek, 1986). Experimental results, however, show that other propagation modes are not uncommon either. For example, Pardoen et al. (2004) observed that double-edge notched tensile plates made of stainless steel, mild steel, 6082-O and NS4 aluminium alloys, brass, bronze, lead, and zinc systematically show a cup-cup fracture profile, for several different plate thicknesses. In addition, recent experiments evidenced a forth type of crack propagation mechanism - nicknamed *crack tip flipping* - where the fracture surface bears clear signs of a slanted crack flipping back and forth 90° during propagation (see e.g. Simonsen and Törnqvist, 2004; El-Naaman and Nielsen, 2013; Nielsen and Gundlach, 2017).

The common perception of crack propagation mechanisms observed in metal plates can be summarized as follows. In plates made of low strength, high strain hardening capacity metals, crack propagation is preceded by severe necking at the crack tip. Void nucleation therefore starts in the middle of the necking zone where the stress triaxiality has the largest value, and this favours a cup-cup crack profile. Plates made of high strength, low strain hardening capacity metals, on the other hand, allow only a limited amount of necking before fracture. As a result, in such plates, plastic deformation localizes in ∼45° shear bands, leading to cup-cone or slanted cracks. Nevertheless, the underlying reasons for different crack initiation/propagation mechanisms are not yet fully understood (see e.g. Pardoen et al., 2004; Tekoğlu and Nielsen, 2019, and references therein). The present paper is devoted to an experimental investigation of the crack propagation mechanisms in commercially pure aluminium plates (Al 1050 H14). Section 2 presents the materials and experimental procedures. Section 3 summarizes the results, which is followed by concluding remarks in Section 4.

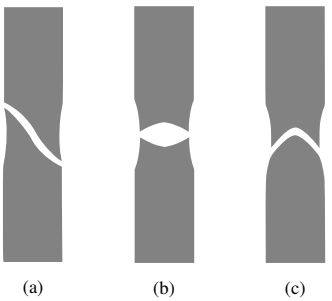

Fig. 1: Schematic showing a (a) slanted, (b) cup-cup, and (c) cup-cone crack propagating toward the reader.

2. Materials and experimental procedures

2.1. Materials

The specimens tested in this study were cut from five different commercially pure aluminium (Al 1050 H14) plates, each plate having a different thickness $t \in \{0.5,\ 1.0,\ 3.0,\ 4.0,\ 5.0\}$ mm. The elemental weight percentages of the plates, which were determined by optical emission spectroscopy, are given in Table 1. Each value in Table 1 represents the average for six different tests. Table 2 presents the mechanical properties of the plates, where E is the Young's modulus, $\sigma_{0.2}$ is the 0.2 percent yield stress, σ_u is the ultimate tensile strength, N and K are respectively the strain hardening exponent and the strength coefficient in the Hollomon's relation:

$$\sigma = K\epsilon^N, \tag{1}$$

with σ and ϵ being, respectively, the true stress and true strain. The parameter called "Direction" in Table 2 denote the loading direction with respect to the rolling direction: 0° (90°) specimens were tested parallel (perpendicular) to the rolling direction. The Young's moduli were measured by impulse excitation and vibration technique, and the remaining mechanical properties were obtained from uniaxial tension tests performed on dog-bone shaped rectangular specimens. The presented N and K values provide the best fit (in a least square sense) of the Hollomon's relation to the experimental tensile stress-strain curves before necking. The plastic properties given in Table 2 correspond to the average values for five dog-bone specimens, which were cut from the aluminium plates by electron discharge machining (EDM).

Table 1: Elemental weight percentages for the Al 1050 H14 plates tested in this study.

Thickness (mm)	Al	Fe	Si	Ti	Cu	Mn	Mg	Zn
0.5	99.4	0.238	0.193	0.0247	0.0026	< 0.001	< 0.0001	< 0.0050
1.0	99.4	0.267	0.206	0.0194	0.0037	< 0.001	< 0.0001	< 0.0050
3.0	99.4	0.283	0.134	0.0242	0.0062	< 0.001	< 0.0001	< 0.0050
4.0	99.4	0.268	0.177	0.0241	0.0046	< 0.001	< 0.0001	< 0.0050
5.0	99.3	0.260	0.097	0.0263	0.0090	< 0.001	< 0.0001	< 0.0050

Table 2: Mechanical properties of Al 1050 H14 plates tested in this study. E is the Young's modulus, $\sigma_{0.2}$ is the 0.2 percent yield stress, σ_u is the ultimate tensile strength, N and K are respectively the strain hardening exponent and the strength coefficient in the Hollomon's relation given Eq. (1). Direction denotes the loading direction with respect to the rolling direction.

Thickness (mm)	Direction	E (GPa)	$\sigma_{0.2}$ (MPa)	σ_u (MPa)	N	K (MPa)
0.5	0°	66.0	106.4	112.0	0.0356	131.9
0.5	90°	66,0	113.2	117.7	0.0339	138.6
1.0	0°	66.0	111.6	116.9	0.0345	137.2
1.0	90°	66.0	118.5	124.8	0.0427	152.7
3.0	0°	69.1	120.3	132.2	0.0507	166.4
3.0	90°	69.1	141.3	145.5	0.0327	170.9
4.0	0°	70.2	110.7	118.4	0.0388	140.3
4.0	90°	70.2	120.7	124.9	0.0322	146.0
5.0	0°	69.8	115.5	121.5	0.0365	144.4
5.0	90°	69.8	122.5	129.5	0.0471	162.3

2.2. Mode I test setups

Two different experimental setups were used to perform Mode I tearing experiments. The first setup, shown in Fig. 2a, is in fact a scaled down version of the setup designed by Simonsen and Törnqvist (2004). This setup was used to test the so-called Edge Crack Specimens (ECS), which were subjected to both tension and in-plane bending as illustrated in Fig. 2b. The initial notch length, $a_0 = 50$ mm, and the width, $w = 200$ mm, of the ECS specimens allow the crack to propagate 30 plate thicknesses for 5 mm-thick samples. The ratio of the crack growth length to the plate thickness increases with decreasing t, reaching a maximum of 300 for $t = 0.5$ mm. The initial height of the ECS specimens, $H_0 = 248$ mm, was observed to be large enough to minimize the influence of the far boundaries, an observation supported by El-Naaman and Nielsen (2013) who used a similar setup to test 2 mm-thick Al 1050 H14 plates. The second setup, shown in Fig. 2c, imposes pure uniaxial tension on Double Edge Notched Tensile (DENT) specimens, as illustrated in Fig. 2d (see also Pardoen et al., 2004; El-Naaman and Nielsen, 2013). For the DENT specimens, the initial notch length is $a_0 = 45$ mm, the initial height is $H_0 = 100$ mm, and the width is $w = 180$ mm. In these samples, two cracks grow toward each other over a 90 mm-ligament connecting the two notches. Both the ECS

(a)

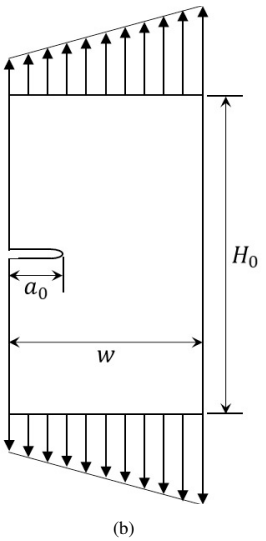

(b)

(c)

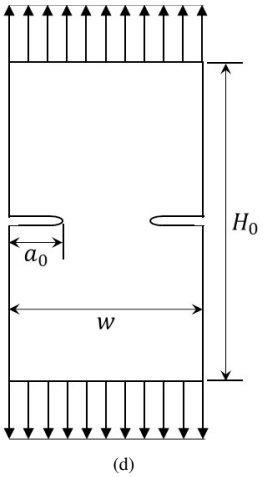

(d)

Fig. 2: The two setups used to perform Mode I tearing experiments in this study: the setup for tearing (a) the Edge Crack Specimens (ECS), and (b) the Double Edge Notched Tension (DENT) specimens. The dimensions for the (c) ECS specimens, which are subjected to combined tension and in-plane bending, are $a_0 = 50$ mm, $w = 200$ mm, and $H_0 = 376$ mm, and for the (d) DENT specimens, which are subjected to pure uniaxial tension, are $a_0 = 45$ mm, $w = 180$ mm, and $H_0 = 220$ mm .

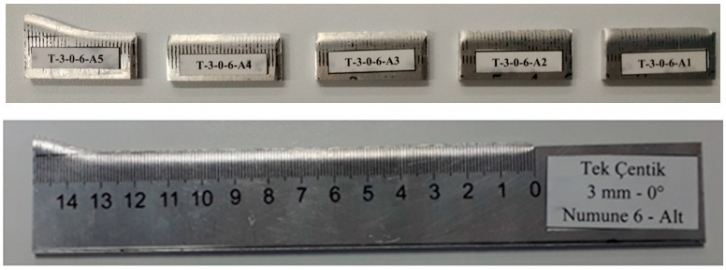

Fig. 3: Five scanning electron microscopy (SEM) samples extracted from the optical microscopy sample below, for an edge crack specimen (ECS).

and the DENT specimens were extracted from the aluminium plates by laser cutting, while the notches were formed by EDM. Note that in 0° (90°) specimens which are loaded parallel (perpendicular) to the rolling direction, the notches align perpendicular (parallel) to the rolling direction.

A minimum of six specimens were tested for each direction-thickness combination, the total number being 74 for the ECS and 72 for the DENT specimens. All the experiments were performed using an Instron 600 LX hydraulic testing machine, under quasi-static loading conditions. Preliminary tests showed that the load-displacement curves for different loading rates between 0.4 mm/s and 1.0 mm/s were essentially coinciding for the ECS specimens. Nevertheless, to avoid any risks, a loading rate of 0.6 mm/s was employed for the ECS specimens, and 0.3 mm/s for the DENT specimens. In order to be able to measure the crack advance, timed still-photographs were taken throughout each test, as shown in Figs. 2a and 2c. The applied displacement and the corresponding force and time were recorded by the testing machine. To facilitate the crack advance measurements, a ruler was drawn on each specimen along the expected crack path by serigraph printing (see Fig. 3). [1] It is well known that the crack initiation has negligible effect on the crack front if the crack is allowed to grow over several specimen thicknesses (see e.g. El-Naaman and Nielsen, 2013), which was the case for all the ECS and DENT specimens. No pre-cracking was therefore performed in this study.

2.3. Fractography

Detailed crack surface morphology analyses were performed using a Scanning Electron Microscope (SEM, FEI XL-40, 20 kV). However, a selection from the large pool of samples was first performed to choose one representative sample for each direction-thickness combination. For this purpose, the fracture surface on one part of all the separated samples were observed by light optical microscopes (Nikon Eclipse LV150N ve Nikon TU Plan Fluor 100x). Fig. 3 shows SEM samples for an ECS, together with one optical microscopy sample (below). Optical microscopy samples, which contain the entire crack, were cut from the specimens by using a guillotine. SEM samples, with a height of approximately 10 mm and a width between 30 to 50 mm, however, were extracted from the optical microscopy samples by EDM, so that they have flat bottom surfaces which allow them to be easily mounted on the SEM stage. All the samples were systematically analysed from a top view to determine the crack surface morphologies.

3. Results

Figures 4 and 5 show the measured force-displacement and force-crack advance curves for 5 mm-thick ECS and DENT specimens, respectively. The results for several different specimens are in good agreement, which is the case for all other specimen thicknesses (not shown here) as well. For the DENT specimens, the crack advance "a" represents the average value for the two cracks propagating toward each other from the two notches located at the opposite edges of the specimen. Extensive crack tunnelling was detected in DENT specimens, while the crack only became visible on the outside surfaces at later stages of the deformation. Due to a limited number of measurements (still photos), the

[1] The heat treatment process normally applied in the last stage of serigraph printing was omitted not to alter the properties of the specimens.

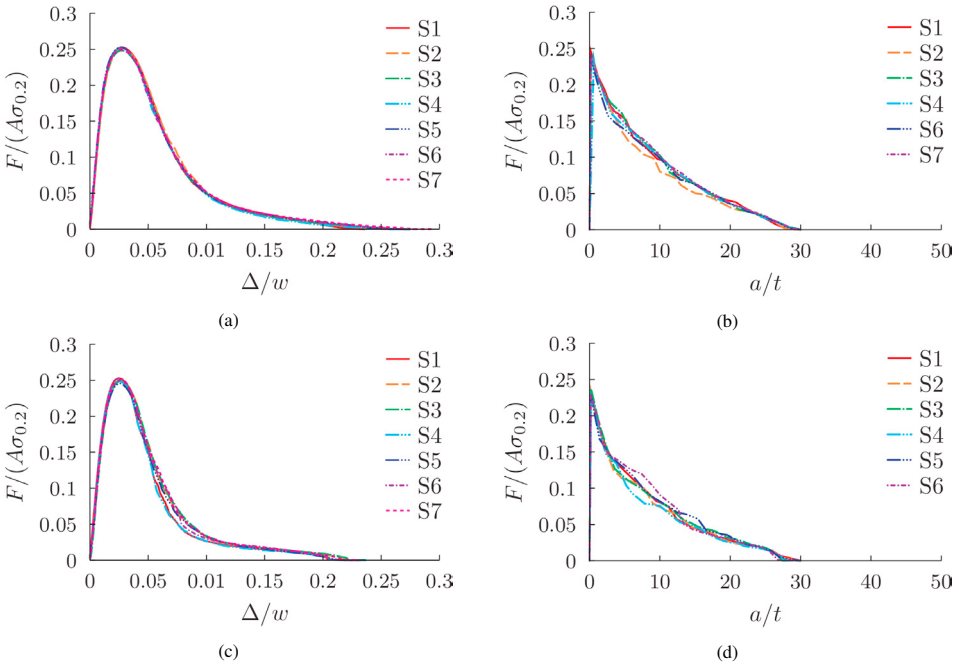

Fig. 4: Measured (a, c) force-displacement and (b, d) force-crack advance curves for 5 mm-thick (a, b) 0° and (c, d) 90° ECS. Δ is the displacement of the loading grips, $w = 200$ mm is the specimen width (see Fig. 2b), $t = 5$ mm is the specimen thickness, a is the crack advance, F is the force, $\sigma_{0.2}$ is 0.2 percent yield stress of the specimen (see Table 2), and the area $A = wt = 1000$ mm^2.

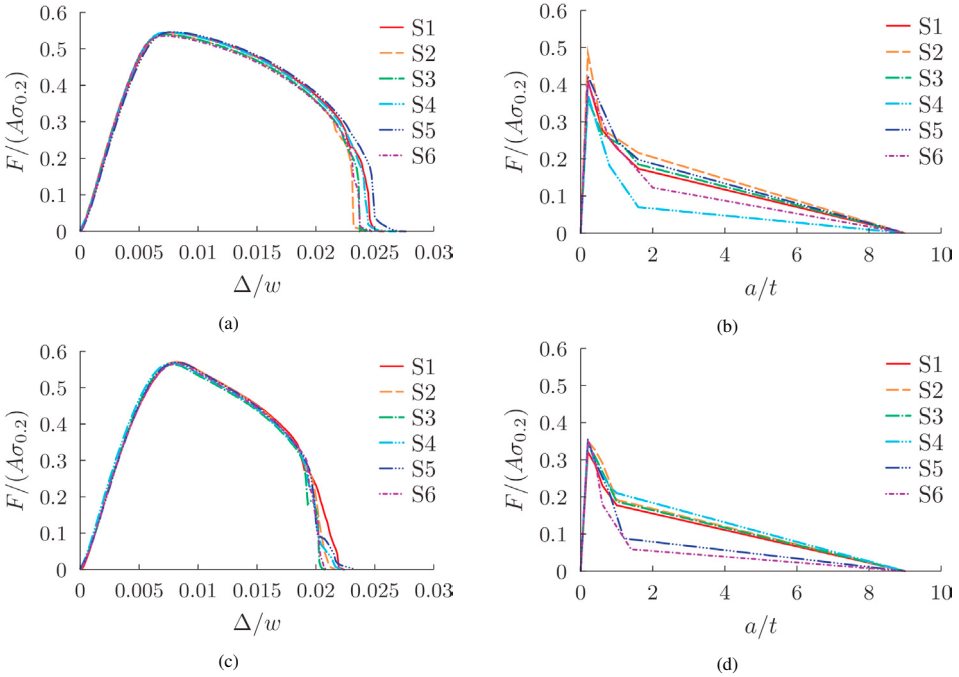

Fig. 5: Measured (a, c) force-displacement and (b, d) force-crack advance curves for 5 mm-thick (a, b) 0° and (c, d) 90° DENT specimens. Δ is the displacement of the loading grips, $w = 180$ mm is the specimen width (see Fig. 2b), $t = 5$ mm is the specimen thickness, a is the crack advance, F is the force, $\sigma_{0.2}$ is 0.2 percent yield stress of the specimen (see Table 2), and the area $A = wt = 900$ mm^2.

cracks appeared as if they suddenly propagated several plate thicknesses on the outside surfaces for these specimens. This tunnelling also partially explains why the differences in the crack advance curves between different samples are relatively large for DENT specimens (see Figs. 5b and 5d). Furthermore, it can be deduced from Figs. 4 and 5 that the normalized total elongation values are slightly larger for 0° samples when compared to 90° samples for each type of specimens (ECS vs. DENT), indicating a slight anisotropic material response. The normalized elongation values corresponding to the normalized peak force values are, however, nearly the same for all 0° and 90° samples. Despite the Mode I loading nature of both the ECS and the DENT test, a profound difference is observed in the load-deflection curves. While the ECS test displays an early peak force and a rather rapid drop in load carrying capacity, the DENT specimen shows a high load carrying capacity after the peak force has been attained. This is tied to the deformation mechanisms at play. In both tests, severe thinning of the plate occurs prior to crack initiation and this thinning stretches across the entire ligament (between the notches) in the DENT test such that the peak force is reached long before crack initiation. This becomes evident when comparing the load-deflection curves (Figs. 5a,c) with the load-crack advance curves (Figs. 5b,d). In contrast, the crack initiation essentially sets-in at peak force in the ECS test (see Fig. 4). Moreover, the crack propagation in the ECS samples take place over a much greater distance making the load-crack extension curves nicely resolved by the limited number of still photos recorded during each test (compare Figs. 4b,d to Figs. 5b,d).

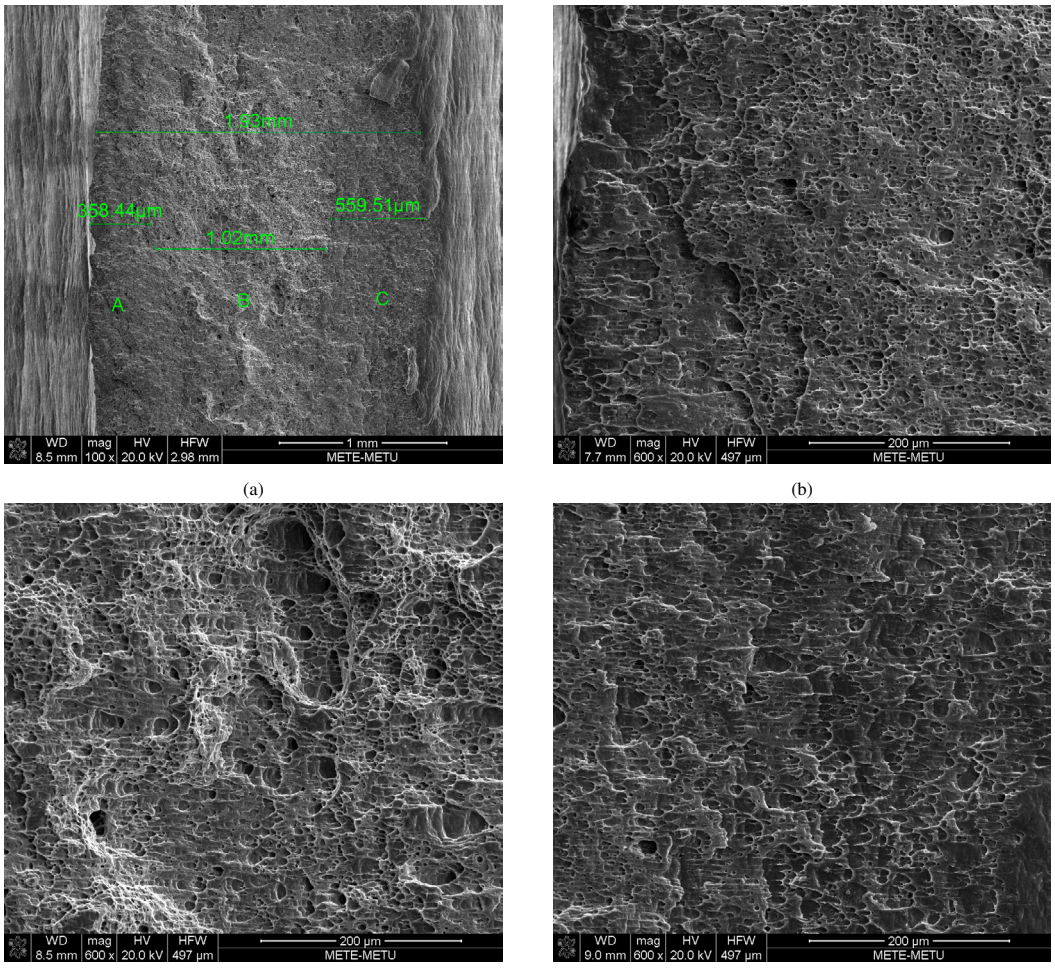

(a) (b) (c) (d)

Fig. 6: (a) A scanning electron fractograph for a 5 mm-thick, 0° DENT specimen exhibiting slanted fracture. The crack is inclined such that the region A has a higher altitude than the region C. The magnified views for the regions (b) A, (c) B, and (d) C.

For the observed crack surface morphologies, the focus here is kept on the DENT specimens, because the overall tendencies were found to be independent of the specimen/setup type; see Table 3. A scanning electron fractograph for a slant crack propagating in a 5 mm-thick, 0° DENT specimen is presented in Fig. 6a, together with the magnified views for three different regions located on the crack surface in Figs. 6b-d. The distinguishing features for a slant crack are: (i) an inclined crack surface (note that the crack surface altitude decreases from the region A toward the region C), (ii) sheared voids (clearly seen in the magnified views, especially for the regions A and C), and (iii) a smaller average void size in comparison to that in a region of cup-cup crack growth (which is also the case for the specimen in Fig. 6a, although not shown here). For all the ECS and DENT specimens, a cup-cup crack morphology exists in the neighbourhood of the notches, where the cracks initiate. For 5 mm-thick specimens, the predominant crack surface morphology is slanted, while a only limited amount of cup-cup crack propagation is observed. For all other specimen thicknesses, on the other hand, the extend of the cup-cup crack profile is considerably larger than that of slanted profile, especially for 0° specimens. In a typical cup-cup crack, there exist a dimpled central zone in between two smooth mirror-like surfaces often referred to as “shear lips”. Fig. 7 shows representative crack surface morphologies for specimen thicknesses below 5 mm. It is worth to notice that these mirror-like fracture surfaces have been observed in earlier published studies, but the underlying failure mechanism remains to be explained.

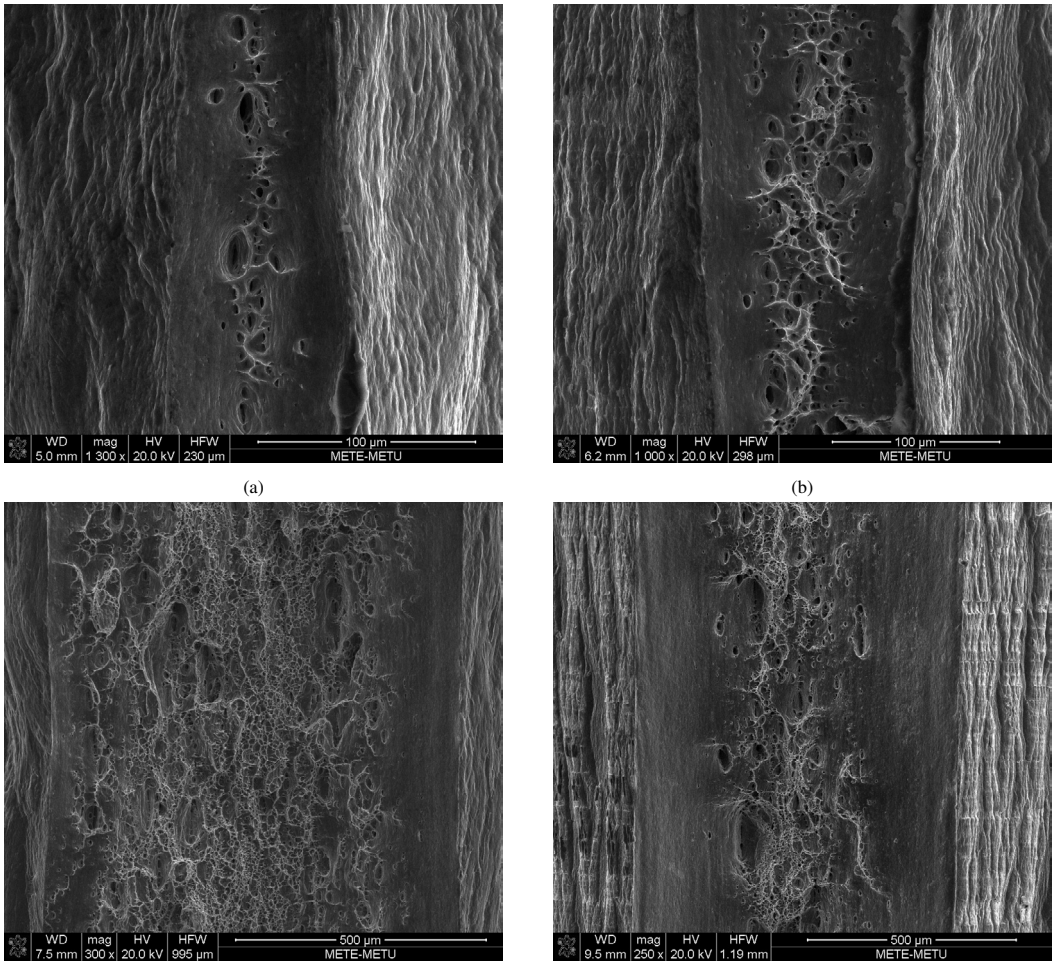

Fig. 7: A scanning electron fractograph for a (a) 0.5 mm-thick, 90°, (b) 1.0 mm-thick, 0°, (c) 3.0 mm-thick, 90°, and (d) 4.0 mm-thick, 0° DENT specimen.

4. Concluding Remarks

The results for crack surface morphologies observed in Al 1050 H14 plates are summarized in Table 3. The crack propagation mechanism is observed to be only a little affected by the specimen/setup types (ECS and DENT), while it clearly depends on the orientation of the loading direction with respect to the rolling direction. The cracks have a tendency to slant for 90° specimens, but the predominant propagation mechanism is still cup-cup for specimens with a thickness below 5 mm. For 0° specimens, which have slightly lower yield and tensile strength values compared to their 90° counterparts (see Table 2), the total elongation (therefore the amount thinning) is relatively larger (see Figs. 4 and 5); this partly explains why the cup-cup profile is more dominant. For 5 mm-thick specimens, however, the cracks slant for both 0° and 90° directions, which implies that the plate thickness have an effect on the crack profile. The fact that the differences in the mechanical properties and chemical compositions of the plates with different thicknesses (see Table 1) are relatively small suggests that damage–related microstructural parameters (such as the identity, volume fraction, morphology, average size, and spatial distribution of void nucleation sites) can have a significant effect on the crack surface morphology. In fact, the properties of the second phase particles (intermetallics) acting as void nucleation sites can be considerably different even for plates with similar chemical compositions, depending on the details of the production process; see e.g. Allen et. al (1998). Future work will be devoted to a thorough investigation of the effects of the plate thickness and intermetallics on the crack propagation mechanisms in commercially pure aluminium (Al 1050 H14) plates.

Table 3: An overview of the crack surface morphologies observed for the ECS and DENT specimens. Direction denotes the loading direction with respect to the rolling direction. Note that for 0° (90°) specimens, the crack propagates perpendicular (parallel) to the lading direction. The morphologies written in bold represent the dominant crack propagation mechanisms.

	ECS		DENT	
Thickness (mm)	0°	90°	0°	90°
0.5	**cup-cup**-slanted	**cup-cup**-slanted	cup-cup	**cup-cup**-slanted
1.0	cup-cup	**cup-cup**-slanted	cup-cup	**cup-cup**-slanted
3.0	cup-cup	**cup-cup**-slanted	cup-cup	**cup-cup**-slanted
4.0	cup-cup	**cup-cup**-slanted	cup-cup	**cup-cup**-slanted
5.0	cup-cup-**slanted**	cup-cup-**slanted**	cup-cup-**slanted**	cup-cup-**slanted**

Acknowledgements

The authors gratefully acknowledge the financial support by TÜBİTAK (Project No: 315M133).

References

Allen, C. M., O'Reilly, K. A. Q., Cantor, B., Evans, P. V. (1998). Intermetallic phase selection in 1XXX Al alloys. Progress in Materials Science, 43, 89–170.

Anderson, T. L., 2005. Fracture Mechanics: Fundamentals and Applications (3. Edition). Boca Raton: CRC Press.

Broek, D., 1986. Elementary Fracture Mechanics (4. Edition). Dordrecht, The Netherlands: Kluwer Academic Publishers.

El-Naaman, S. A., Nielsen, K. L., 2013. Observations on Mode I ductile tearing in sheet metals. European Journal of Mechanics A/Solids, 42, 54–62.

Irwin, G. R., Kies, J. A., Smith, H. L., 1958. Fracture strengths relative to onset and arrest of crack propagation. American Society for Testing and Materials (ASTM) Transactions, 58, 640–60.

Knott, J. F., 1973. Fundamentals of Fracture Mechanics. London: Butterworths.

Lecarme, L., Tekoğlu, C., Pardoen, T. 2011. Void growth and coalescence in ductile solids with stage III and stage IV strain hardening. International Journal of Plasticity, 27, 1203–23.

Li, W., Siegmund, T., 2002. An analysis of crack growth in thin-sheet metal via cohesive zone model. Engineering Fracture Mechanics, 69, 2073–93.
Nielsen, K. L., Gundlach, C., 2017. Crack tip flipping under mode I tearing: Investigated by X-ray tomography. International Journal of Solids and Structures, Volume 118, 119–127.
Pardoen, T., Hachez, F., Marchioni, B., Blyth, P. H., Atkins A. G., 2004. Mode I fracture of sheet metal. Journal of the Mechanics and Physics of Solids, 52, 423–52.
Pardoen, T., Scheyvaerts, F., Simar, A., Tekoğlu, C., Onck, P. R., 2010. Multiscale modeling of ductile failure in metallic alloys. Comptes Rendus Physique, 11, 326–45.
Rivalin, F., Pineau, A., Di Fant, M., Besson, J., 2001. Ductile tearing of pipeline-steel wide plates - I. dynamic and quasi-static experiments. Engineering Fracture Mechanics, 68, 329–345.
Scheyvaerts, F., Onck, P. R., Tekoğlu, C., Pardoen, T., 2011. The growth and coalescence of ellipsoidal voids in plane strain under combined shear and tension. Journal of the Mechanics and Physics of Solids, 59, 373–97.
Simonsen, B., Törnqvist, R., 2004. Experimental and numerical modelling of ductile crack propagation in large-scale shell structures. Marine Structures, 17, 1–27.
Tekoğlu, C., 2015. Void coalescence in ductile solids containing two populations of voids. Engineering Fracture Mechanics, 147, 418–430.
Tekoğlu, C., Hutchinson, J. W., Pardoen, T., 2015. On localization and void coalescence as a precursor to ductile fracture. Philosophical Transactions of the Royal Society A373: 20140121.
Tekoğlu, C., Leblond, J.-B., Pardoen, T., 2012. A criterion for the onset of void coalescence under combined tension and shear. Journal of the Mechanics and Physics of Solids, 60, 1363–81.
Tekoğlu, C., Nielsen, K. L., 2019. Effect of damage-related microstructural parameters on plate tearing at steady state. European Journal of Mechanics - A/Solids, https://doi.org/10.1016/j.euromechsol.2019.103818.
Tekoğlu, C., Pardoen, T., 2010. A micromechanics based damage model for composite materials. International Journal of Plasticity, 26, 549-69.
Tvergaard, V., Needleman, A., 1984. Analysis of the cup-cone fracture in a round tensile bar. Acta Metallurgica, Volume 32, 157–169.
Ugural, A. C., 2009. Stresses in Beams, Plates, and Shells (3. Edition). New York: CRC Press.
Ventsel, E., Krauthammer, T., 2001. Thin Plates and Shells: Theory, Analysis, and Applications. New York: Marcel Dekker, Inc.